Structural properties of BeTe/ZnSe superlattices

T. Walter, A. Rosenauer, R. Wittmann, and D. Gerthsen
Laboratorium für Elektronenmikroskopie, Universität Karlsruhe, Kaiserstraße 12, D-76128 Karlsruhe, Federal Republic of Germany

F. Fischer, T. Gerhard, A. Waag, and G. Landwehr
Physikalisches Institut der Universität Würzburg, Am Hubland, D-97074 Würzburg, Federal Republic of Germany

P. Schunk and T. Schimmel
Institut für Angewandte Physik, Universität Karlsruhe, Kaiserstraße 12, D-76128 Karlsruhe, Federal Republic of Germany

(Received 15 July 1998)

The structural properties of BeTe/ZnSe short-period superlattices grown by molecular-beam epitaxy on (001)-oriented GaAs substrates were investigated. Different growth modes were used which influence the morphology and chemical transition at the interfaces. The BeTe/ZnSe superlattices were examined by optical microscopy, conventional and high-resolution transmission electron microscopy, x-ray diffractometry, and atomic force microscopy, with a particular emphasis on the defect generation mechanisms and the effects of different bond configurations at the interfaces. The critical thicknesses largely exceed the theoretical values for the plastic relaxation by misfit dislocations. The mismatch is relaxed by cracks preferentially oriented along one particular ⟨110⟩ direction under tensile stress conditions. In order to quantify the abruptness of the chemical transition at the interfaces and to determine the layer thicknesses accurately, high-resolution transmission electron micrographs were evaluated by correspondence analysis. [S0163-1829(99)10111-5]

I. INTRODUCTION

Due to their high-band-gap energies, beryllium-chalcogenides are considered to be promising materials for optoelectronic devices in the green and blue spectral region. The atomic bonding in the BeTe crystal has a more covalent character compared to most other wide-band-gap II-VI semiconductors like ZnSe, where the ionicity of the atomic bonding is larger.[1] This leads to a considerable increase of the elastic hardness. A higher covalency is expected to improve the degradation behavior of II-VI laser diodes emitting in the blue-green region of the visible spectrum.[2]

Binary BeTe and ZnSe are almost lattice matched to GaAs. The lattice parameters of GaAs, BeTe, and ZnSe are $a_{\mathrm{GaAs}}=5.654$ Å, $a_{\mathrm{BeTe}}=5.626$ Å, and $a_{\mathrm{ZnSe}}=5.668$ Å at room temperature.[3] If the mismatch is defined as $f:=(a_s-a_f)/a_f$ (a_s and a_f are the lattice parameters for the substrate and the film), the corresponding lattice misfits with respect to the GaAs substrate are $f_{\mathrm{ZnSe}}=-2.5\times10^{-3}$ and $f_{\mathrm{BeTe}}=+5.0\times10^{-3}$. Therefore, ZnSe and BeTe can be combined in BeTe/ZnSe superlattices (SL's) on GaAs substrates with alternating tensile and compressive strain. If the layer thickness ratio between BeTe and ZnSe is adjusted close to $\frac{1}{4}$ (taking into account the different elastic properties of the ZnSe and BeTe), lattice match with respect to the GaAs substrate can be obtained.

In the present study the structure of BeTe/ZnSe SL's was characterized with different experimental techniques because the understanding of the defect generation is essential for the use of superlattices in light-emitting devices. The chemical composition of the interface regions was varied by special molecular-beam-epitaxy (MBE) growth techniques which are outlined in Sec. II. Particular emphasis was put on the determination of the strain state of the superlattice, the observed defects, the assessment of the layer undulations, and the width and chemical composition at the interfaces. The experimental results are described in Sec. III which is subdivided into Secs. III A (sample morphology), III B (polarity determination), and III C (a determination of the width of the chemical transition by the correspondence analysis). The effects leading to the observed microstructure and nanostructure are considered in Sec. IV. It will be shown that the chemical composition at the interfaces of the short-period superlattices plays an important role because it influences the average lattice parameter and consequently the strain and the structural and electronic properties.

II. EXPERIMENTAL TECHNIQUES

Three BeTe/ZnSe SL's with 75 (sample *A*) and 25 (samples *B* and *C*) periods were grown by MBE on GaAs(001) at a substrate temperature of 300 °C. The GaAs substrates were prepared by growing a 300-nm-thick GaAs buffer layer at 580 °C. Each period of the SL nominally consists of 4-ML BeTe and 10-ML ZnSe. The samples were specifically grown to modify the bond configuration at the interfaces.

Sample *B*, with interfaces containing predominantly ZnTe bonds, was grown by the following procedure. ZnSe was deposited on BeTe by first closing the Be shutter, waiting for 5 sec then closing the Te-shutter and opening the Zn shutter immediately, and finally after 3 sec opening the Se shutter. A corresponding cycle was applied for the BeTe on ZnSe transition by first closing the Se shutter, waiting 4 sec and opening the Te shutter and closing the Zn shutter, and opening the Be shutter after another delay of 4 sec.

For sample *C* with BeSe-rich interfaces the following growth sequence was used. For the ZnSe on BeTe interface

 ©1999 The American Physical Society

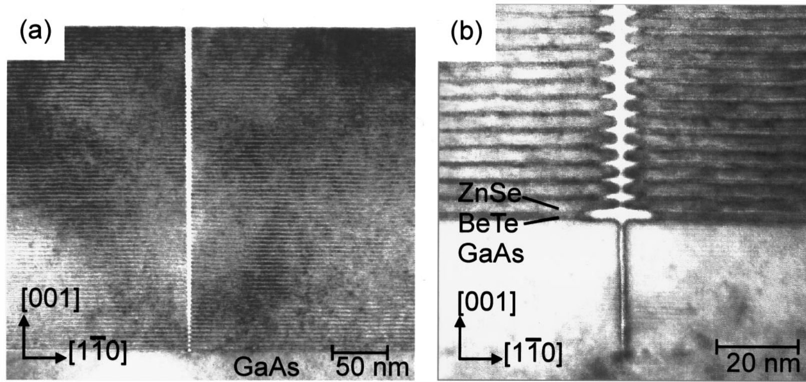

FIG. 1. Cross-sectional TEM images along the [110] direction of sample *A*. (a) $\mathbf{g}=(004)$ two-beam bright field image displaying a V-shaped crack in the SL. (b) HRTEM image of another crack showing the area close to the GaAs/SL interface with undulating crack edges.

the Be and Te shutters were closed simultaneously with the opening of the Se shutter. After a Se flux of 5 sec the Zn shutter was opened. The opposite sequence was performed for the growth of the BeTe on ZnSe transition, but only with a Se flux of 4 sec. The two shutters for the corresponding binary components were simultaneously closed and opened for sample *A*.

For a visual surface inspection of the SL's, Nomarski high-contrast microscopy was used. Atomic force microscopy (AFM) was performed with a commercial instrument (Park Scientific Instruments) and a home-built AFM head equipped with a laser beam deflection detection system in ambient air at room temperature using a V-shaped silicon nitride cantilever with a pyramidal tip.

The transmission electron microscopy (TEM) investigations were carried out with plan-view and cross-sectional specimens along the two ⟨110⟩ projections with a Philips CM 200 FEG/ST electron microscope. The preparation of the samples started with the standard mechanical thinning procedure with grinding and dimpling. To minimize preparation-induced defects, a low acceleration voltage of 3 kV, low currents of 0.5 mA, and liquid-nitrogen cooling was applied for the Ar^+-ion milling.

The x-ray measurements were performed using a Philips X'PERT System. The average composition of the superlattice was obtained by an iterative fit procedure for the rocking curve of the (002) and (004) reflections. The EPITAXY program (Philips version 1.2c) was used with the BeTe and ZnSe layer thicknesses obtained by the correspondence analysis as starting values for the fit.

III. EXPERIMENTAL RESULTS

Different structural aspects were studied whose results are presented in the following subsections.

A. Superlattice morphology

In Fig. 1(a), a cross-sectional TEM micrograph of sample *A* with a SL thickness of 320 nm is presented, that contains a V-shaped crack whose width increases toward the surface. In the two orthogonal ⟨110⟩ projections, crack distances of 1–3 μm were found. The shape of the crack is typical for all observed cracks. The crack in Fig. 1(a) terminates at the GaAs/SL interface, but some cracks penetrate into the substrate up to a depth of 30 nm as shown in the high-resolution transmission electron microscopy (HRTEM) image [Fig. 1(b)]. The width of the cracks at the surface of the SL varies between 3 and 6 nm.

Figure 1(b) reveals undulating crack edges with a smaller crack width between the ZnSe layers. The wavy crack edges are attributed to artifacts of the specimen preparation procedure. The exposure of the crack surface to oxygen after the MBE growth or to water during the sample preparation could induce the growth of oxides. Beryllium is known to have a large hydration enthalpy[4] and a strong tendency to oxidization. The oxide is highly strained on the BeTe, and could be preferentially removed during the Ar^+-ion milling.

A slight concave curvature of the SL layers between the cracks is visible on larger sections of HRTEM images which indicates the presence of tensile strain. As steps could not be observed in HRTEM micrographs, the interface of the GaAs substrate with the SL was confirmed to be flat on an atomic scale for 50 nm. Misfit dislocations were observed neither in cross-sectional nor in plan-view specimens (electron transparent area $>10^{-3}\,cm^2$), indicating that the dislocation density must be smaller than $10^3\,cm^{-2}$.

A cross-sectional TEM image along one ⟨110⟩ projection of sample *B* is shown in Fig. 2(a). The total thickness of the SL is 120 nm. The substrate/SL interface shows an undulation with a period in the order of 100 nm and an amplitude of about 5–10 ML which prevails through the whole BeTe/ZnSe SL structure. Such an undulation could not be observed by TEM investigations along the perpendicular ⟨110⟩ projection, where the interface appeared essentially smooth. Structural defects in sample *B* were not observed in cross-sectional TEM. The planview TEM examination yielded only one misfit dislocation in a TEM specimen with an electron transparent area of more than $1.5\times10^{-3}\,cm^2$ corresponding to a dislocation density $<10^3\,cm^{-2}$.

Figure 2(b) shows a ⟨110⟩ HRTEM micrograph which was taken from sample *C*. In this case, the thickness of the whole SL is about 100 nm. Figure 2(b) reveals numerous stacking faults and microtwins lying in the two different visible {111} planes. Cross-sectional TEM investigations of a specimen along the perpendicular ⟨110⟩ projection showed the same defects with a comparable density.

In Figs. 3(a), 3(b), and 3(c), Nomarski micrographs of samples *A, B*, and *C* are presented. The surfaces of all samples are characterized by a cross-hatched line pattern. By atomic force microscopy, small ribbons with a width of about 1–3 μm (the density of the ribbons is greater than

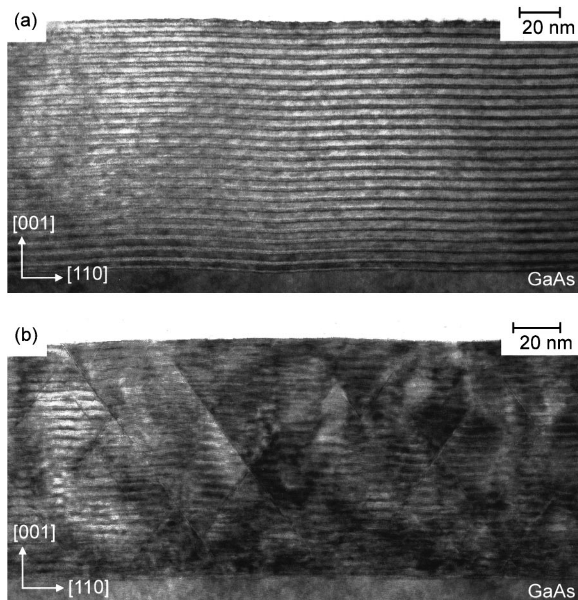

FIG. 2. Cross-sectional TEM images of ⟨110⟩-oriented specimens of (a) sample *B* and (b) sample *C* taken along the ⟨110⟩-zone axis orientation.

10^7 cm^{-2}), separated by steps with a height smaller than 1 nm, were observed which are responsible for the cross-hatched contrast in the optical microscopy. A cross-hatched pattern with the same appearance was found on the surface of a GaAs substrate covered only with the GaAs buffer layer. An additional feature of sample *A* is the presence of cracks that are preferentially oriented along only one ⟨110⟩ direction. The crack separation ranges between 2 and 50 μm, in contrast to the crack density and orientations in the TEM cross-section samples. After a cleaning treatment in ultrasonically vibrated acetone the AFM investigations revealed a surface with a crack density in the order of 1–3 μm for both ⟨110⟩ directions. Samples *B* and *C* with the thinner BeTe/ZnSe SL's do not show any cracks.

B. Crystal polarity

In the case of sample *A*, the crystal polarity was determined using convergent beam electron diffraction (CBED) because of the observed asymmetry of the relaxation by cracks. In compound semiconductors the two orthogonal ⟨110⟩ directions are not equivalent. The difference is depicted in Fig. 4 for the example of GaAs where the arrangement of the gallium and arsenic reverses in the closely spaced dumb-bell atoms along the [110] and $[1\bar{1}0]$ directions. The polarities are deduced from the convention of Gatos and Lavine,[5] where the $(\bar{1}\,\bar{1}\,\bar{1})$ surface is terminated with group-V atoms.

The polarity of the ⟨110⟩ direction of the cracks was determined by the following CBED technique which was suggested by Taftø and Spence.[6] A cross-sectional specimen oriented along the [110] direction is tilted by approximately 10° along the (002) Kikuchi band with $\mathbf{g}=(002)$. Two bright HOLZ (higher-order Laue zone) lines cross each other under a flat angle [marked with black arrows in Fig. 5(b)] in the (002) CBED disk if the Bragg condition is fulfilled for the

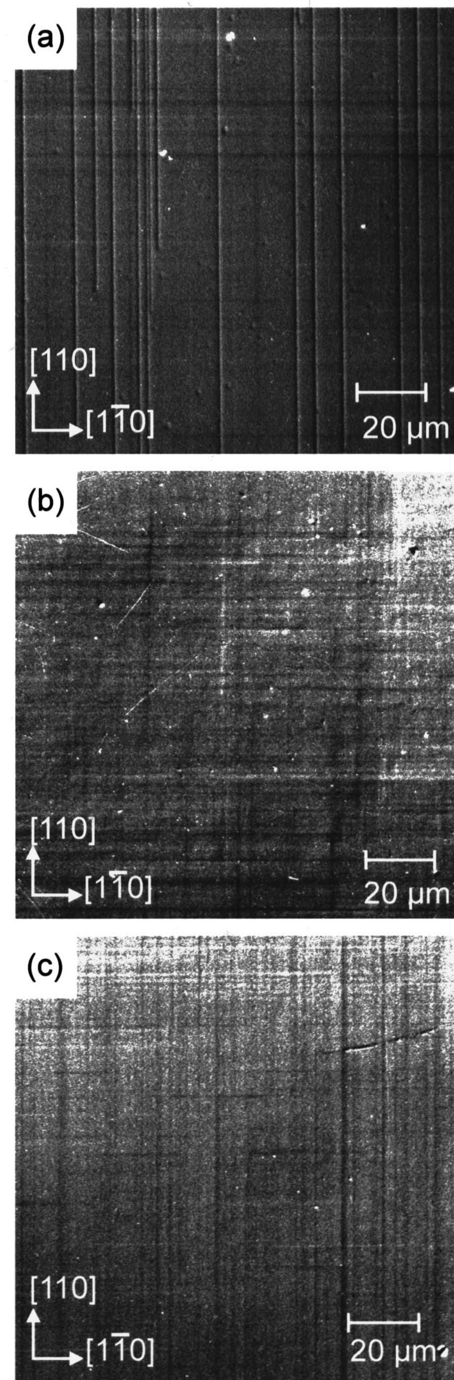

FIG. 3. Nomarski high-contrast micrographs of the surface morphologies of (a) sample *A*, (b) sample *B*, and (c) sample *C* showing cross-hatched patterns. In addition, the surface of sample *A* exhibits cracks oriented along the [110] direction.

(002), $(\bar{1}1\bar{9})$, and $(\bar{1},1,11)$ reflections [$(\bar{1}1\bar{9})$ and $(\bar{1},1,11)$ are the HOLZ lines in the (002) disk]. Tilting the sample until the Bragg condition is fulfilled for the $(00\bar{2})$, $(\bar{1}19)$, and $(\bar{1},1,\overline{11})$ reflections, two dark lines cross each other in the $(00\bar{2})$ CBED disk [Fig. 5(c)]. The exact electron-beam direction can now be determined by comparing one of these CBED images with the accompanying cross-sectional TEM image, containing the (001) surface of the GaAs substrate [Fig. 5(a)]. This first requires the determination of the image

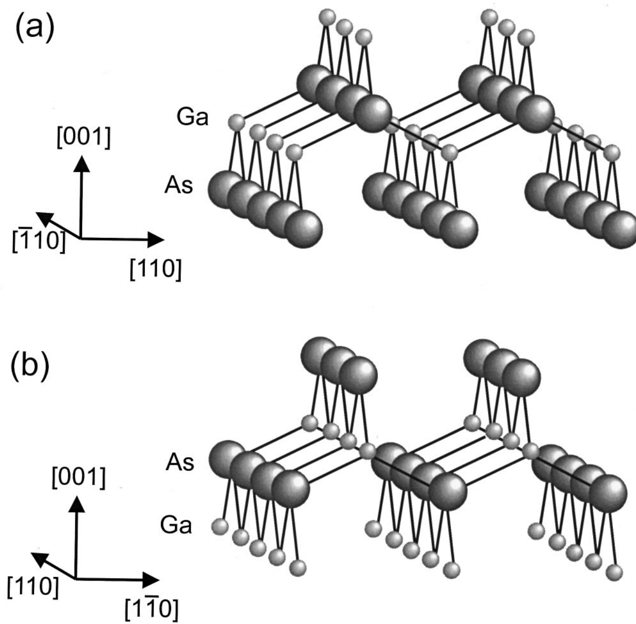

FIG. 4. GaAs structure along the [110] and [1 1̄ 0] directions.

rotation between the diffraction pattern and the TEM micrograph of a specimen with known crystal polarity. The orientation of the CBED images toward the TEM image for a GaAs sample with a [110] viewing direction is summarized in Fig. 5. For a sample with [1 1̄ 0] orientation, the directions in the CBED pattern are reversed. The BeTe and ZnSe layers of the SL are assumed to be of comparable polarity to the substrate, i.e., the positions of the group-VI atoms correspond to the arsenic locations. It was deduced from the CBED analysis that the cracks of sample *A* are preferentially oriented along the [110] direction.

C. Correspondence analysis

In order to determine the abruptness of the chemical transition at the interface regions and accurate layer thicknesses, HRTEM images of cross-sectional specimens along the ⟨110⟩ projection were analyzed using the correspondence analysis[7] (CA) which was implemented in the DALI software package.[8] The HRTEM negatives were digitized with a CCD camera at a resolution of 1024×1024 picture elements (pixels). The CA is a special variant of the multivariate statistics (MS). A raw description of the method is given in the case of the evaluation of sample *A*, which is outlined in the flow chart (Fig. 6).

The dark areas in Fig. 6(a) correspond to the BeTe layers, and the bright regions to the ZnSe. The digitized image was subdivided into $N=33\times 70$ image unit cells as shown in the upper left corner of Fig. 6(a). The image unit cells that may differ in their sizes and shapes are transformed into quadratic cells of identical size of $P=2^n\times 2^n$ ($n\in\mathbb{N}$, typically $n=5$) pixels. The corresponding procedure is described in detail by Rosenauer *et al.*[9] Each image unit cell is represented by a P-dimensional positive and real vector r_j ($j=1,\ldots,N$) which contains the intensity of each pixel. The aim of the *MS* is the investigation of the shape of the cloud of points formed by the tips of the N image vectors. This problem is analogous to the well-known task of finding the axis of least inertia of a distribution of N points of the mass m_j, where m_j is given here by the integral intensity of the unit cell j. Therefore, the origin of the coordinate system is shifted into the center of the mass distribution by an axis transformation. The given problem is solved by calculating eigenvalues λ_k ($k=1,\ldots,M$) and eigenvectors e_k of the matrix of inertia. Each eigenvector e_k represents a principal axis of the cloud of image points r_j. The main idea of this method is that only a small number M of principal axes is sufficient to describe the given distribution of points r_j. It can be shown that the corresponding M eigenvectors are eigenvectors $e_{\alpha_1}\ldots e_{\alpha_M}$ to the M largest eigenvalues $\lambda_{\alpha_1}>\lambda_{\alpha_2}>\cdots>\lambda_{\alpha_M}$. These eigenvectors can be rearranged into unit cells which are now called eigencells. In Fig. 6(b) the first three eigencells are presented, which were obtained from the first three eigenvectors. In the present case it was found that the first eigenvector e_{α_1} contains the characteristics of the contrast pattern of the BeTe region. This behavior is shown in Fig. 6(c), where the projections of each image unit cell onto the first eigencell (given by the scalar product of the two vectors $r_j\cdot e_{\alpha_1}$) are arranged in a map. The different gray levels of the rectangles in this map represent the degree of correspondence of each unit cell with the first eigencell. Bright rectangles that label good correspondence belong to the BeTe region. In contrast, the dark cells represent the ZnSe. The image given in Fig.

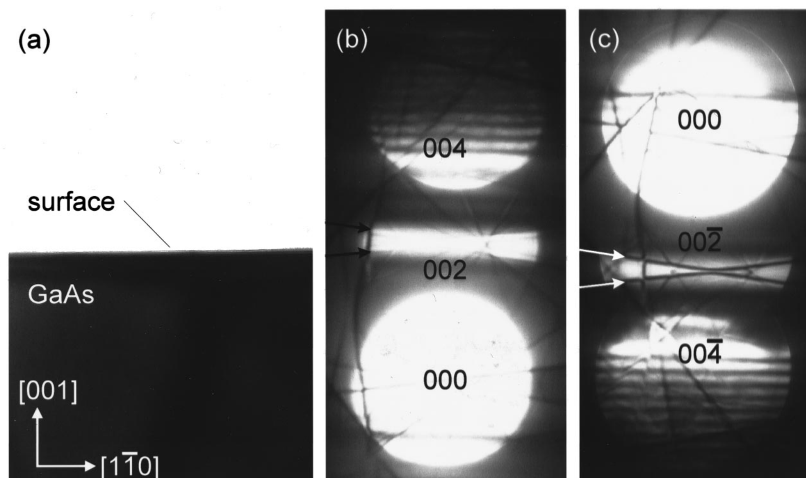

FIG. 5. CBED images for the determination of the crystal polarity. (a) Cross-sectional image of a GaAs(001) surface along the [110] viewing direction. (b) Orientation of a CBED image with the (002) Bragg reflection containing the two crossing bright HOLZ lines (arrows). (c) Corresponding orientation of a CBED image containing the (00$\bar{2}$) spot with the two crossing dark HOLZ lines (arrows). The image rotation was corrected to orient (a)–(c) along the same direction.

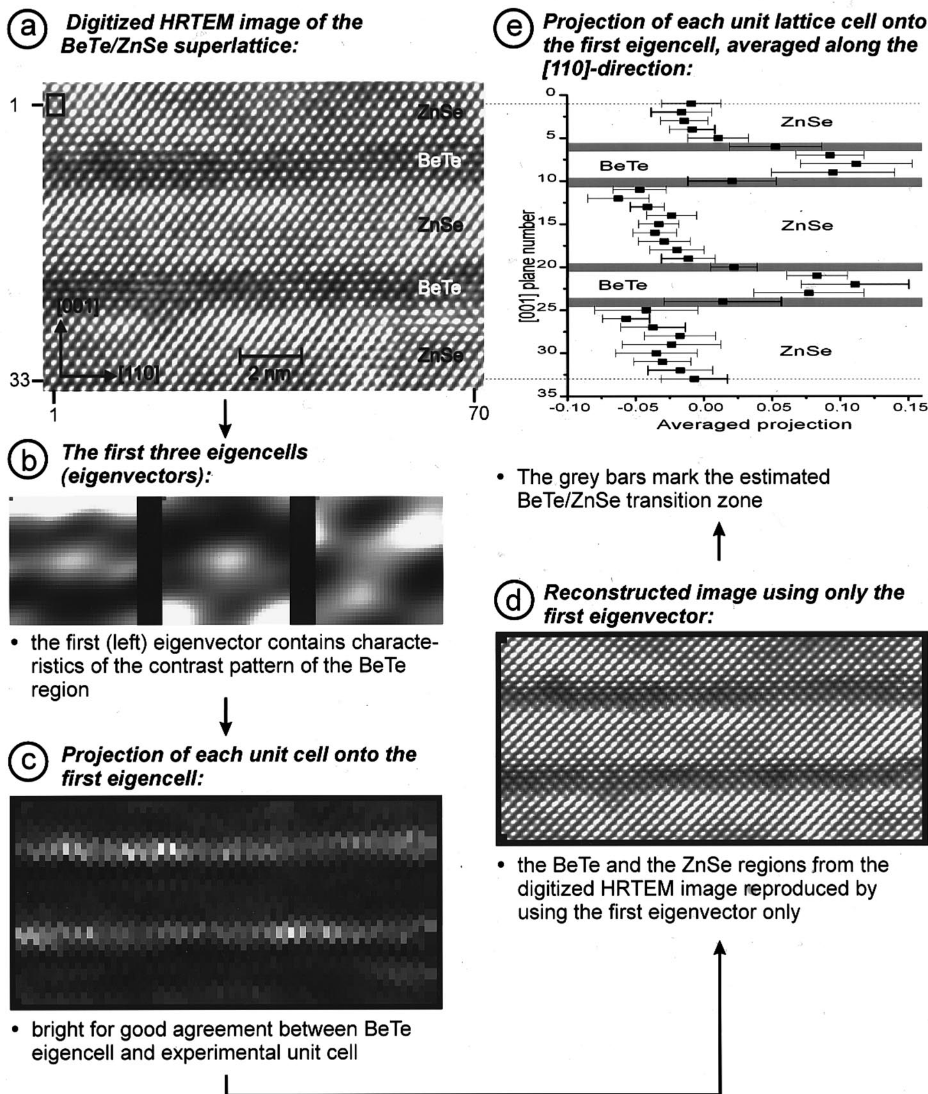

FIG. 6. Schematic drawing showing the successive steps of the correspondence analysis. (a) Digitized HRTEM image of the BeTe/ZnSe SL (sample *A*). (b) The first three eigencells. (c) A map showing the projection of each image unit cell onto the first eigencell. (d) A reconstruction of (a) using only the first eigencell. (e) The projection of each image unit cell onto the first eigencell averaged along the ⟨110⟩ direction, plotted vs the monolayer numbers in the [001] direction.

6(d) is a reconstruction of Fig. 6(a) using only the first eigencell. A diagram, where the values of $r_j \cdot e_{\alpha_1}$ averaged along the [110] direction is plotted versus the monolayer number, is depicted in Fig. 6(e) opposite to the digitized HRTEM image [Fig. 6(a)]. The gray bars in this plot mark the estimated transition zone from BeTe to ZnSe. Its width is about one atomic layer at each layer boundary. The layer thicknesses can be accurately measured, which yields 3 ML of BeTe, 9 ML of ZnSe, and 2 ML for the transition zones of each SL period.

The same analysis procedure was carried out with samples *B* and *C*. The corresponding results are shown in Fig. 7. In the case of sample *B* [Fig. 7(a)], a period of 17 ML with 7-ML BeTe, 8-ML ZnSe, and a transition zone of 1 ML at each interface were measured. In Fig. 7(b) the results for sample *C* are presented. The SL has a period of 14 ML, which is in agreement with the nominal value. The transition regions in this SL structure are rather broad. The thicknesses of the BeTe and ZnSe layers were determined to be 3 and 5 ML. Broad chemical transition zones of 3 ML were measured at the interfaces.

The width of the transition regions determined by the CA is not only dependent on the real chemical transitions. In addition, this value comprises effects of layer undulations along the direction of the electron beam and along the [110] direction due to the averaging by the CA analysis which has to be considered.

In the case of sample *B*, the averaging of the projections along 1 ML leads to a broadening of the transition zone because of the undulations which is visible in Fig. 2(a). A step of 1 ML was attributed to the undulation which is recognized in Fig. 7(a) by comparing corresponding arrows at the left and right sides of the image. Therefore, the width of the transition region can be estimated to be less than 1 ML.

IV. DISCUSSION

In Secs. IV A–IV C the aspects of the strain relaxation and the effects of the interface growth modes on the width of the chemical transition will be discussed for the three samples. Finally, suggestions concerning the origin of the cross-hatched pattern on the superlattice surfaces will be made in Sec. IV D.

A. Sample *A*

The morphology of sample *A* is dominated by the cracks and their asymmetrical densities along the [110] and $[1\bar{1}0]$

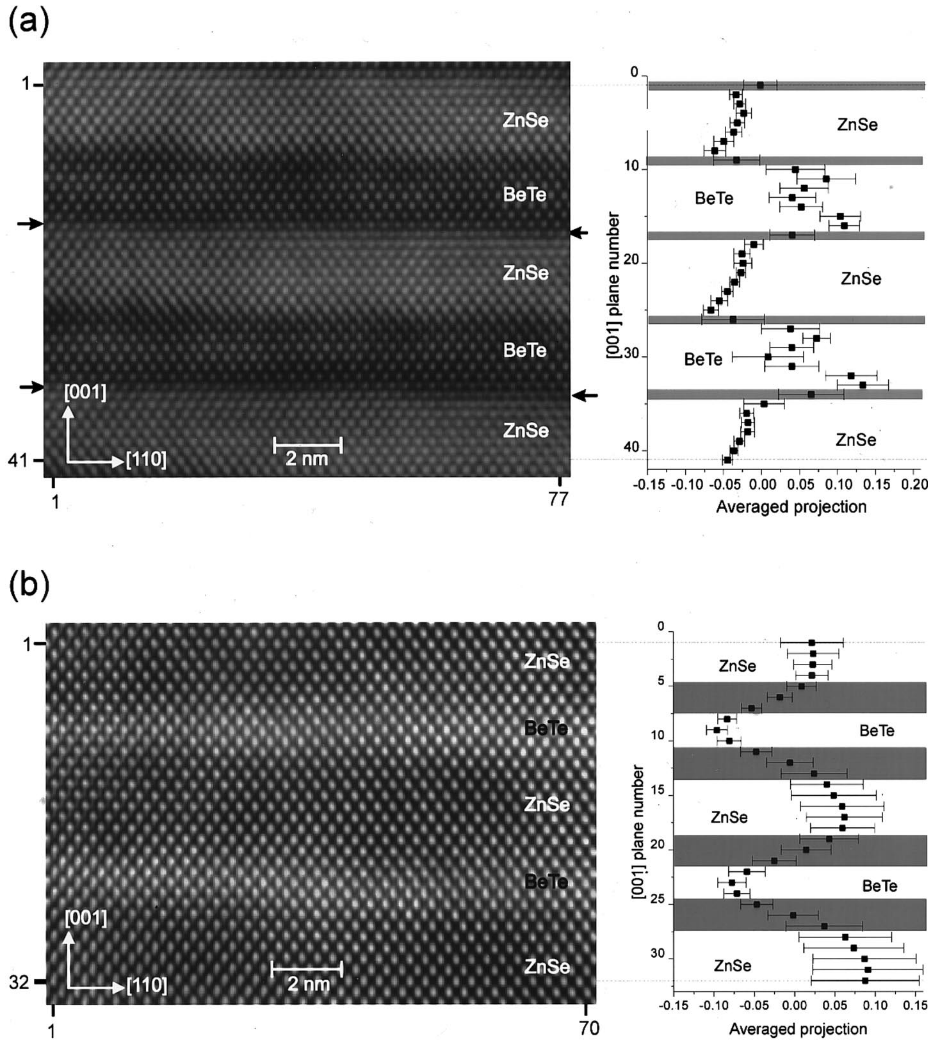

FIG. 7. Correspondence analysis with digitized HRTEM image and the projection of each image unit cell onto the first eigencell, averaged along the ⟨110⟩ direction for (a) sample B and (b) sample C.

directions. The cracks result from the misfit stress in the superlattice induced by the GaAs substrate. To understand the microstructure, the critical thicknesses for the relaxation by misfit dislocations and cracks are calculated. This task is accomplished by approximating the superlattice by a homogeneous layer with an average SL lattice parameter a_{SL}, which is deduced from the individual BeTe and ZnSe layer thicknesses. This approximation is justified because the layer thicknesses of the BeTe and ZnSe are distinctly smaller than the critical thickness for the relaxation between the individual layers,[10] which is experimentally verified by the fact that misfit dislocations are not observed at the interfaces in the SL.

The relevant lateral lattice parameter of the SL for the misfit relaxation processes is calculated according to Eq. (1),[10] which contains the shear moduli G_{BeTe} and G_{ZnSe} and the individual layer thicknesses t_{BeTe} and t_{ZnSe}:

$$a_{\mathrm{SL}}=\frac{G_{\mathrm{BeTe}}a_{\mathrm{BeTe}}t_{\mathrm{BeTe}}+G_{\mathrm{ZnSe}}a_{\mathrm{ZnSe}}t_{\mathrm{ZnSe}}}{G_{\mathrm{BeTe}}t_{\mathrm{BeTe}}+G_{\mathrm{ZnSe}}t_{\mathrm{ZnSe}}}. \quad (1)$$

The shear moduli $G=(C_{11}-C_{12})/2$ are yielded with the elastic constants C_{ij}. For ZnSe, $C_{11}=8.95\times10^{10}\,\mathrm{N/m^2}$ and $C_{12}=5.39\times10^{10}\,\mathrm{N/m^2}$ are taken from Ref. 3, which leads to a shear modulus $G_{\mathrm{ZnSe}}=1.78\times10^{10}\,\mathrm{N/m^2}$. For BeTe a shear modulus of $G_{\mathrm{BeTe}}=3.4\times10^{10}\,\mathrm{N/m^2}$ was calculated with $C_{11}=11.1\times10^{10}\,\mathrm{N/m^2}$ and $C_{12}=4.3\times10^{10}\,\mathrm{N/m^2}$ from first-principles calculations in Ref. 11. A lateral lattice parameter a_{SL} of 5.650 Å is calculated with the measured BeTe/ZnSe ratio of 4/10, which is nearly lattice matched with respect to the GaAs substrate. In contrast, the presence of tensile stress is required for the formation of cracks in an epitaxial film.[12,13] This discrepancy is resolved by considering the bond configuration at the interface. A tensile stress is achieved if the effect of the BeSe bonds with $a_{\mathrm{BeSe}}=5.139$ Å at the transition regions is taken into account which induces a significant reduction of a_{SL} in short-period superlattices. For the layer thicknesses of the CA with 1-ML BeSe at each transition as initial parameters for the fit of the rocking curve, a SL with a period of 13.77 ML could be adapted, comprising an average layer composition corresponding to 10.07-ML ZnSe, 0.35-ML BeSe, 3.00-ML BeTe, and another 0.35-ML BeSe. This result shows that the simultaneous opening and closing of the shutters during the growth of sample A leads to BeSe-rich interfaces, which is attributed to a displacement of Te by Se atoms and the high sticking coefficient of the Be.[14]

The relevant lateral lattice parameter of the SL was finally calculated by extending Eq. (1) to three different layers. With the refined composition scheme, $a_{\mathrm{SL}}(A)=5.601$ Å is obtained, with $G_{\mathrm{BeSe}}=4.5\times10^{10}\,\mathrm{N/m^2}$ ($C_{11}=14.9\times10^{10}\,\mathrm{N/m^2}$ and $C_{12}=5.9\times10^{10}\,\mathrm{N/m^2}$ according to Ref. 11).

A relation between the critical thickness h_c for the relaxation by misfit dislocations and the lattice mismatch f was given by Matthews and Blakeslee.[15] The expression of Matthews and Blakeslee can be simplified without significant loss of accuracy according to People and Bean,[16] where h_c is given by

$$h_c \cong \frac{b}{4\pi f(1+\nu)}\left[\ln\left(\frac{h_c}{b}\right)+1\right], \tag{2}$$

with the Poisson ratio ν $[\nu = C_{12}/(C_{11}+C_{12})]$ and the length of misfit dislocation Burgers vector b. Equation (2) was deduced from mechanical equilibrium theory which is known to underestimate the actual critical thicknesses up to one order of magnitude depending on the barriers toward dislocation nucleation which was shown by People and Bean[16] for SiGe layers on Si(001) substrates. However, the calculation of h_c is only intended to serve as an estimate for the expected relaxation by misfit dislocations. For sample A with a misfit of $f=0.95\%$ a critical thickness of 10 nm is computed which is much smaller than the total SL thickness of 320 nm even if h_c is distinctly underestimated.

An expression for the critical thickness of crack generation was proposed in Ref. 12,

$$t_c = \frac{\Gamma(1-\nu)}{G(1+\nu)f^2}, \tag{3}$$

where Γ is the {110} surface energy of the epilayer. Since the surface energies for the Be chalcogenides have not been known up to now, the ZnSe values of Γ, ν, and G are taken with $\Gamma_{\mathrm{ZnSe}} = 0.87\ \mathrm{J/m^2}$ (Oshcherin[17]) for an estimation of t_c. This leads to a critical thickness of approximately 250 nm, which is smaller than the total SL thickness of 320 nm. Due to the significantly increased elastic hardness of the Be chalcogenides compared to ZnSe, the experimental critical thickness could be reduced by more than 100 nm.

Although the critical thickness for the misfit dislocation generation is largely exceeded, the mismatch is only relaxed by cracks. Therefore, a strong barrier for the dislocation generation must exist. Since it is known that misfit dislocations are easily nucleated and mobile in mismatched ZnSe/GaAs heterostructures[18] the observed effect can be attributed to the BeTe. In addition, the stress distribution in the superlattice could be a barrier toward the misfit dislocation propagation, because the dislocations experience a repulsive force in the compressively strained ZnSe. Also, the considerable difference between the elastic constants of the BeTe and ZnSe must be taken into account because a difficulty in moving a dislocation out of the soft material into the hard material can be expected.[19]

Three different mechanisms were suggested in Ref. 12 for the crack nucleation. As a first possibility, 90° dislocations at or near the SL/substrate interface, formed by the interaction of two 60°-type dislocations on two intersecting {111} glide planes, could act as stress concentration centers enabling crack nucleation. The origin of the crack asymmetry may be explained by the different mobilities of the α and β dislocations on the corresponding $\{111\}_A$ and $\{111\}_B$ glide planes. The determination of the crystal polarity showed that almost all cracks are oriented along the [110] direction. This would indicate a higher mobility of the β dislocations, which is in contradiction to the observed higher mobility of the α dislocations in ZnSe.[18] To our knowledge, measurements of the BeTe-dislocation mobilities do not exist. The second possibility also relies on an asymmetrical misfit dislocation density. If the mismatch is first relaxed by misfit dislocations along the $[1\bar{1}0]$ direction with a larger dislocation mobility, the strain along the orthogonal [110] direction prevails which induces a higher probability of crack nucleation along this orientation. This model would indeed be consistent with a higher mobility for α dislocations, in contrast to the first model. However, dislocation-induced processes for the crack nucleation are in general highly unlikely because the dislocation density is much lower than the crack density.

Steps at the SL/substrate interface running along the [110] or $[1\bar{1}0]$ directions were also considered in Ref. 12 as an alternative source for the generation of cracks. The steps induce a lattice mismatch parallel to the step edge, which could induce a stress concentration along the step.

For sample A an additional possibility for the crack nucleation can be suggested. The steps at the SL surface resulting in the cross-hatched pattern could lead to stress concentrations at the surface. From the high density of cracks after the treatment in ultrasonically vibrated acetone, it must be supposed that only a small amount of mechanical stress is sufficient for the crack generation after the critical thickness for crack nucleation is exceeded. Therefore, the asymmetry of the crack density in sample A is attributed to a unilateral external stress, e.g., while removing the specimen from the MBE holder to which it was mounted with indium. The comparable crack density for both orthogonal ⟨110⟩ projections, which was found in the cross-sectional specimen, is most likely caused by the stress exerted on the sample during the mechanical thinning procedure.

B. Sample *B*

Sample B, with ZnTe-rich interfaces, is compressively strained according to the x-ray diffraction (XRD). The excess of ZnTe bonds ($a_{\mathrm{ZnTe}} = 6.104$ Å) at the interfaces causes a significant increase of the average lattice parameter. With the results of the CA as initial values for the fit of the rocking curve, a SL with a period of 17.61 ML could be adapted with an average layer composition of 8.27-ML ZnSe, 0.75-ML ZnTe, 7.82-ML BeTe, and another 0.75-ML ZnTe. The intrinsic lattice parameter of sample B could accordingly be calculated with $G_{\mathrm{ZnTe}} = 1.56\times 10^{10}\ \mathrm{N/m^2}$ ($C_{11} = 7.22\times 10^{10}\ \mathrm{N/m^2}$ and $C_{12} = 4.09\times 10^{10}\ \mathrm{N/m^2}$[23]) to be $a_{\mathrm{SL}}(B) = 5.666$ Å, which corresponds to a misfit of about -0.21%.

A critical thickness for the misfit dislocation generation of 67 nm is calculated according to Eq. (2), which is significantly below the total SL thickness of 120 nm. The TEM investigations of sample B yield a very small dislocation density below $10^3\ \mathrm{cm^{-2}}$, indicating that the SL is almost pseudomorphic with respect to the GaAs substrate. A strong barrier for the dislocation generation is present in sample A. Although sample B is in a compressive strain state (as opposed to sample A), the same mechanisms can be assumed to be responsible for the inhibited dislocation nucleation. The layer undulation of sample B along the [110] direction is

likely to be induced by a miscut of the GaAs wafer and/or the preparation of the GaAs substrate prior to the buffer layer growth.

C. Sample *C*

The correspondence analysis of sample *C* revealed a diffuse chemical transition extending over about 3 ML, in contrast to the interface widths of samples *A* and *B*, which are in the order of one atomic layer. The following explanation could account for the difference between the samples. BeSe bonds were observed to be preferably formed in sample *A* if the shutters are simultaneously opened and closed. By offering excess Be and Se at the interfaces, the concentration of the BeSe is expected to increase, which leads to ternary and quaternary compounds extending into the adjacent ZnSe and BeTe layers. A fit of the rocking curve was not possible for sample *C*, because the composition is likely to vary across the whole transition zone.

The stacking faults in sample *C* are assumed to originate from a Se surface coverage of the substrate material. With the presence of Se at the GaAs surface, the Ga atoms have a high tendency to form Ga_2Se_3, which was shown to be a source for the generation of the stacking faults in the epitaxial ZnSe layers.[20]

D. Surface morphology

A cross-hatched surface morphology was frequently reported in III-V-homoepitaxy and heteroepitaxy,[21,22] where a direct correlation was found between the density of misfit dislocations and the cross-hatched lines. The lines were not observed after the start of the growth, but appeared after exceeding the critical layer thickness. Heun *et al.*[23] investigated the surface morphology of MBE-grown ZnSe, which was either directly deposited on a GaAs(001) substrate or on an $In_xGa_{1-x}As$ buffer layer (a GaAs buffer layer was grown on each substrate). A cross-hatched pattern was only visible directly on the surface of the partially relaxed $In_xGa_{1-x}As$ layer, and on the strained ZnSe surface grown on this buffer layer. They found that the ZnSe layer only replicates the surface morphology of the underlying $In_xGa_{1-x}As$ buffer. Cross hatching was not observed on the ZnSe layers grown directly on the GaAs buffer.

The TEM investigation of samples *A* and *B* yielded dislocation densities smaller than $1\times10^3\ cm^{-2}$, which is more than one order of magnitude less than the surface step density. Therefore, a correlation between the cross-hatched pattern and misfit dislocations is unlikely. However, the surface of the GaAs buffer already shows a cross-hatched pattern. The step structure at the BeTe/ZnSe SL surface can therefore be assumed to be a reproduction of the step structure on the GaAs buffer layer surface similar to the effect observed by Heun *et al.*[23] for ZnSe. A comparable effect is observed for the undulations at the GaAs surface along the [110] direction in sample *B*, which is likewise reproduced through the whole BeTe/ZnSe SL. The most likely origin of the cross-hatched pattern on the GaAs buffer layer surface are slip lines by dislocation generation and motion induced by thermal stresses. The GaAs buffer and the SL are grown in different chambers which requires a temperature reduction to almost room temperature between the deposition of the buffer and the SL.

V. CONCLUSION

Short-period BeTe/ZnSe SL's with different bond configurations at the interfaces were grown by MBE and characterized with different microscopical methods and XRD. It was shown that the strain state of the SL's is strongly influenced by the different shear moduli, and that the bond configurations at the interfaces play an important role in short-period superlattices. X-ray-photoemission spectroscopy measurements of the valence-band offsets yielded a large shift of 0.8 eV,[24] revealing the effect of the strain and interface chemistry on the electronic properties.

Correspondence analysis turned out to be a valuable evaluation method to quantify the information contained in HRTEM images regarding the abruptness of the chemical transition and the layer thicknesses of superlattices. Abrupt chemical transition regions are achieved if the shutters are simultaneously opened and closed during the MBE and under ZnTe-rich conditions, while an excess of Be and Se leads to chemically diffuse interfaces. It was shown that the results of the correspondence analysis are well suited as starting values for the fit of the rocking curves to obtain quantitative values for the average composition of the SL's.

The surfaces of the SL's exhibited a cross-hatched pattern of surface ribbons, separated by steps with a height of less than 1 nm which are oriented along the two orthogonal ⟨110⟩ directions. A correlation between the cross-hatched pattern at the SL surfaces and the misfit dislocation density could not be established.

A strong barrier for the generation of dislocations in BeTe/ZnSe SL's exists, because a misfit dislocation density smaller than $10^3\ cm^{-2}$ was found although the critical thickness for the generation of misfit dislocations is largely exceeded. The tensile strain in SL *A* induced the formation of cracks which are oriented preferentially along the [110] direction. The most likely origin are the steps at the GaAs/SL interface or at the SL surface acting as stress concentration centers in combination with a unilateral external stress exerted during the handling of the sample after the growth.

ACKNOWLEDGMENTS

We are pleased to acknowledge the support of this project by the Deutsche Forschungsgemeinschaft under Contract No. Ge 841/1.

[1] C. Vèrié, in *Semiconductor Heteroepitaxy, Growth, Characterization and Device Application*, edited by B. Gil and R.-L. Aulombard (World Scientific, Singapore, 1995), p. 73.
[2] A. Waag, F. Fischer, H. J. Lugauer, Th. Litz, J. Laubender, U. Lunz, U. Zehnder, W. Ossau, T. Gerhardt, M. Möller, and G. Landwehr, J. Appl. Phys. **80**, 792 (1996).
[3] *Semiconductors Physics of Group IV Elements and II–VI Compounds*, edited by O. Madelung, Landolt-Börnstein, New Series, Group III, Vol. 17, Pt. b (Springer, New York, 1982).
[4] R. J. Meyer, in Beryllium, Gmelins Handbuch der anorganischen Chemie, Vol. 26 (Verlag Chemie, Weinheim, 1930).
[5] H. C. Gatos and M. C. Lavine, J. Electrochem. Soc. **107**, 427 (1960).
[6] J. Taftø and J. C. H. Spence, J. Appl. Crystallogr. **15**, 60 (1982).
[7] J. F. Aebersold, P. A. Stadelmann, and J.-L. Rouvière, Ultramicroscopy **62**, 171 (1996).
[8] A. Rosenauer, S. Kaiser, T. Reisinger, J. Zweck, and W. Gebhardt, Optik (Stuttgart) **102**, 63 (1996).
[9] A. Rosenauer, T. Remmele, D. Gerthsen, K. Tillmann, and A. Förster, Optik (Stuttgart) **105**, 99 (1996).
[10] J. W. Matthews and A. E. Blakeslee, J. Cryst. Growth **32**, 265 (1976).
[11] M. González-Díaz, P. Rodríguez-Hernández, and A. Muñoz, Phys. Rev. B **55**, 14 043 (1997).
[12] R. T. Murray, C. J. Kiely, and M. Hopkinson, Philos. Mag. A **74**, 383 (1996).
[13] P. Franzosi, G. Salviati, M. Scaffardi, F. Genova, S. Pellegrino, and A. Stano, J. Cryst. Growth **88**, 135 (1988).
[14] F. Fischer, G. Landwehr, Th. Litz, H. J. Lugauer, U. Zehnder, Th. Gerhard, W. Ossau, and A. Waag, J. Cryst. Growth **175/176**, 532 (1997).
[15] J. W. Matthews and A. E. Blakeslee, J. Cryst. Growth **27**, 118 (1974).
[16] R. People and J. C. Bean, Appl. Phys. Lett. **47**, 322 (1985).
[17] B. N. Oshcherin, Phys. Status Solidi **34**, K181 (1976).
[18] A. Rosenauer, T. Reisinger, F. Franzen, G. Schütz, B. Hahn, K. Wolf, J. Zweck, and W. Gebhardt, J. Appl. Phys. **79**, 4124 (1996).
[19] D. H. Ghista and W. D. Nix, Mater. Sci. Eng. **3**, 293 (1968).
[20] L. H. Kuo, L. Salamanca-Riba, B. J. Wu, G. M. Haugen, J. M. DePuydt, G. Hofler, and H. Cheng, J. Vac. Sci. Technol. B **13**, 1694 (1995).
[21] K. H. Chang, R. Gibala, D. J. Srolovitz, P. K. Bhattacharya, and J. F. Mansfield, J. Appl. Phys. **67**, 4093 (1990).
[22] Y. Morishita, G. Goto, Y. Nomura, M. Tamura, T. Isu, and Y. Katayama, Jpn. J. Appl. Phys. **33**, L9 (1994).
[23] S. Heun, J. J. Paggel, L. Sorba, S. Rubini, R. Lantier, M. Lazzarino, B. Bonanni, A. Franciosi, J.-M. Bonard, J.-D. Ganière, Y. Zhuang, and G. Bauer, J. Appl. Phys. **83**, 2504 (1998).
[24] M. Nagelstraßer, H. Dröge, F. Fischer, T. Litz, A. Waag, G. Landwehr, and H.-P. Steinrück, J. Appl. Phys. **83**, 4253 (1998).